Original Research

S. Garré*
I. Coteur
C. Wongleecharoen
T. Kongkaew
J. Diels
J. Vanderborght

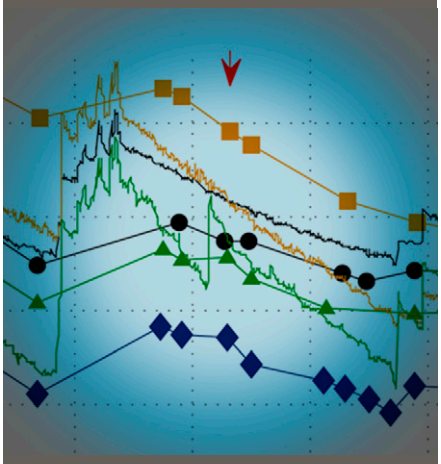

Electrical resistivity tomography can be used to monitor soil moisture depletion under field conditions and with multiple plants. We showed that even though there are limitations arising from soil heterogeneity and dry measurement conditions, important knowledge about spatial and temporal patterns of water depletion can be obtained.

S. Garré, I. Coteur, and J. Diels, KULeuven, Earth and Environmental Sciences, Celestijnenlaan 200, 3000 Leuven, Belgium. S. Garré, presently at Université de Liège, Gembloux Agro-Bio Tech, Passage des Déportés 2, 5030 Gembloux, Belgium. C. Wongleecharoen, Universität Hohenheim, Institute of Plant Production and Agroecology in the Tropics and Subtropics, 70593 Stuttgart, Germany. T. Kongkaew, Kasetsart Univ., Dep. of Soil Science, deceased. J. Vanderborght, Forschungszentrum Jülich, Agrosphere (IBG-3), 52425 Jülich, Germany. *Corresponding author (sarah.garre@ulg.ac.be).

Vadose Zone J.
doi:10.2136/vzj2012.0129
Received 4 Sept. 2012.
Open Access Article

Noninvasive Monitoring of Soil Water Dynamics in Mixed Cropping Systems: A Case Study in Ratchaburi Province, Thailand

Agriculture on shallow or steep soils in the humid tropics often leads to low resource use efficiency. Contour hedgerow intercropping systems have been proposed to reduce run-off and control soil erosion. However, competition for water and nutrients between crops and associated hedgerows may reduce the overall performance of contour hedgerow systems. Electrical resistivity tomography (ERT) is a valuable technique used to assess the distribution and dynamics of soil moisture noninvasively. In this study, we demonstrated its potential to measure soil water depletion in the field in distinct cropping patterns in Ratchaburi province, Thailand. The measurements showed that the soils of our experimental plots were very heterogeneous both along the slope as with depth. This observation highlighted some constraints of the ERT method for soil moisture monitoring in the field, such as the difficulty of defining a relationship between electrical conductivity and soil moisture in very heterogeneous soils. Nevertheless, spatial analysis of the data revealed contrasting water depletion patterns under monocropping and intercropping systems. In this way, ERT provides access to information about the vadose zone moisture dynamics that would be unavailable with classical soil moisture measurements.

Abbreviations: BC, boundary condition; ERT, electrical resistivity tomography; RMSE, root-mean-square error; TDR, time domain reflectometer; TDS, total dissolved solids.

Large areas of the warm, humid tropics in Southeast Asia, the Pacific, Latin America, the Caribbean, and Africa are hilly or mountainous. The combination of steep slopes, highly erosive rainfall, and shallow soils in many areas of the humid tropics makes on-site soil erosion and off-site sedimentation major concerns (Craswell et al., 1997). Contour hedgerow intercropping systems have been promoted in such areas since they are highly effective in reducing erosion (Lal, 1989, Morgan, 2004, Sun et al., 2008). Contour hedgerow intercropping is an agroforestry system, which involves planting hedgerows of perennial shrubs along the contour lines of a slope (Sun et al., 2008, Tang, 2000). Crops are produced in the alleys between the hedgerows. The shrubs have to be pruned regularly to prevent shading and if leguminous shrubs are used, the foliage can provide high-protein forage or nutrient-rich mulch. Next to the main advantage of reducing runoff and erosion, leguminous hedgerows also have a favorable effect on the soil fertility (Danso et al., 1992, Hairiah et al., 2000b, Högberg and Kvarnström, 1982, Imo and Timmer, 2000). Additionally, intercropping represents a risk reduction for the farmer by diversification and less chance of yield loss by pests and diseases (Craswell et al., 1997). Some authors even mention the potential complementarity of the root systems of the different crops, resulting in a more efficient water and nutrient use (Narain et al., 1998).

Nevertheless, many authors also report negative effects of the hedgerow on the main crop (Aerts et al., 1991, Agus et al., 1997, Dercon et al., 2006, Hairiah et al., 2000a, Pansak et al., 2007, Pansak et al., 2008). These negative effects are mostly attributed to competition for nutrients and/or water and are very often only based on comparison of growth and yield performance between monocropped and intercropped plots or fields. Experimental data on the short and long-term effects of contour hedgerow systems on the water and nutrient fluxes are very rare. Hairiah et al. (2000a) quantified overall C and N flows by analyzing soil and plant samples in Sumatra, Indonesia. Pansak et al. (2007) used ^{13}C isotopic discrimination, in combination with standard methods for determining N availability and uptake, to better understand whether or not stress occurred due to nutrient or water deficits in hedgerow intercropping systems in Loei province, Thailand. Pansak et al. (2008) used

resin cores to assess whether leaching of nitrogen occurred in the same field experiment. There are very few studies (Everson et al., 2009, Hauser et al., 2005) reporting spatial and temporal monitoring of water fluxes in hedgerow intercropping systems, even though competition for water is mentioned as a potential drawback in a large number of research articles.

To get a more detailed understanding of the competition for water, two- or three-dimensional monitoring of the water fluxes in the soil–plant–atmosphere system is necessary. Given the potentially high spatial variability of soil moisture in contour hedgerow intercropping systems on steep slopes, a measurement technique with a high spatial resolution must be found. Geophysical imaging techniques, such as electrical resistivity tomography (ERT), may fulfill these requirements. ERT has been used before to observe nonsteady state phenomena in the soil–plant continuum and, more specifically, to observe agricultural crops (Amato et al., 2009, Beff et al. (2012), Cassiani et al., 2012, Garré et al., 2011, Michot et al., 2003, Michot et al., 2001, Srayeddin and Doussan, 2009, Werban et al., 2008). These studies confirm the promising possibilities offered by ERT, but also mention difficulties to interpreting the measured electrical resistivity, particularly under field conditions. Soil bulk resistivity depends on multiple variables, including soil texture, and structure, stone content, soil moisture content, pore water salinity, temperature, and sometimes on the root biomass present. The variability of these factors needs to be restricted or measured independently, to be able to derive soil moisture content from bulk electrical resistivity using a pedo-physical relation. In addition, monitoring of sudden, rapid changes in the vadose zone (e.g., infiltration after a rain event) and spatially variable processes (e.g., root water uptake) require high spatial and temporal resolution. This resolution can only be achieved if the experimental design is optimized to capture the expected types of variation and if the data quality is good. Garré et al. (2012) tested the performance of different ERT electrode arrays to detect soil moisture dynamics in mono- and intercropping systems using virtual experiments. In the current paper, we will use the findings of this previous work to perform a field experiment in Ratchaburi province, Thailand.

The objective of this study was to quantify patterns and strategies of water uptake in space and time of various crops in a contour hedgerow intercropping system with electrical resistivity tomography (ERT). To achieve this, we will (i) derive structural information about the soil profile from the ERT images, (ii) compare spatial and temporal patterns of water depletion between different cropping patterns and crops, and (iii) calculate spatial statistics that summarize and quantify patterns of water depletion.

Materials and Methods

Field Site

The field site is located in the Queen Sirikit Research Station, Ratchaburi Province, Thailand near the village Ban Bo Wi (13°28′8.20″N lat, 99°16′0.20″E long). According to Khedari et al. (2002), the climate is tropical and the site is located in temperature and relative humidity zone 2 (16–38°C, 41–100% RH) The soil of the field site is heterogeneous and ranges between an endoleptic Alisol (hyperdistric, endoskelletic) and hyperskelletic Leptosol (eutric, siltinovic) (according to FAO/ISRIC/ISSS, 1998).

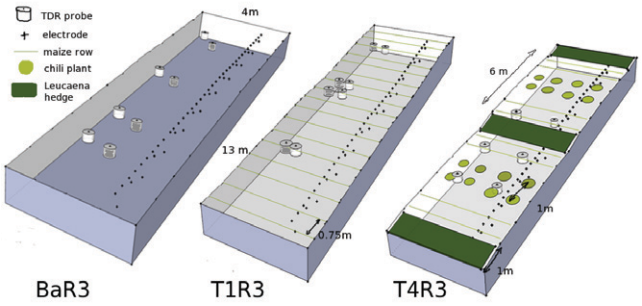

Fig. 1. Overview of cropping patterns Ba, T1 and T4 in replication block 3: time domain reflectometer (TDR) probe location (white: z = 0–0.25 m, gray = 0.20–0.45 m), electrode locations, topography, crops and planting distances. The maize rows contained 16 plants. T6 is similar to T4, but without TDR probes and with the electrodes at the left side of the plot.

The field site consists of three replication blocks (R) in which six agricultural treatments (T) are tested in field plots of 13 m by 4 m. In R3, an additional bare control plot (Ba) was introduced. The plots of R3 (see Fig. 1) are located on sloping land (slope 18–20%) and the soil condition is closest to the Leptosol. The following treatments were used for noninvasive soil moisture monitoring purposes:

Ba: Field plot with bare soil.

T1: Field plot with only Maize (*Zea mays* L. 'Pacific 999') (monocropping) with application of conventional tillage techniques and fertilizer use.

T4: Field plot with Maize rows intercropped with high value chilies (*Capsicum annuum* L. 'Super Hot'), application of minimum tillage and use of fertilizer. Jackbean [*Canavalia ensiformis* (L.) DC] is sown during the dry season as relay and catch crop substituting maize after harvest. In the plot, an additional perennial hedge of *Leucaena leucocephala* (Lam.) de Wit is planted between the rows.

T6: As T4 but without fertilizer application.

The Leucaena hedges were established in 2009 (2 yr before the measurements reported in this paper were performed) and were regularly pruned to avoid shading of the crops (three times during the measurement period: 26 July,13 Aug., and 7 Sept. 2011). The maize was sown and the chilies transplanted on 26 June 2011. We applied the fertilizers as urea, triple super phosphate, and potassium chloride to maize plants at the rate of 62–11–36 kg N–P–K ha^{-1} and only urea to chili plants at the rate of 184–0–0 kg N–P–K ha^{-1}.

Data Acquisition

Field Equipment

The test site was equipped with a weather station, which registered air temperature, relative humidity, solar radiation, wind speed, and rainfall. Soil moisture was continuously logged with time domain reflectometer (TDR) probes distributed over the plots in all replications at 0–0.25 m and 0.20–0.45-m depth. The TDRs were made of two 0.25-m long rods with an inter-rod distance of 0.025 m. The TDR probes were connected to SDMX50 multiplexers, controlled by a TDR100 unit and the data were logged using the CR10X logger (Campbell Scientific Lt., UK). Soil moisture was obtained from the apparent dielectric constant using Topp's equation (Topp et al., 1980). From 20 July to 29 July 2011, we measured the soil temperature at 0.20-, 0.30-, 0.40-, 0.50-, and 0.60-m depth using ECH2O-TE sensors (Decagon devices, Inc., USA) to determine the damping depth of the soil, from which the thermal diffusivity was derived.

The electrical resistivity tomography (ERT) measurements of this study took place from 25 July(DOY 206) to 15 Sept. 2011, which was within the growing season of the crops. Three additional temperature sensors were installed in the topsoil ($z = -0.05$ cm) of R3 and collected data during this period: one under maize cover, one under chili cover, and one under Leucaena cover. Additionally, plant height and leaf area index (LAI) were regularly measured. At the end of the growing season, the root distribution of maize and, if present, Leuceana, in treatments T1, T4, and T6 were measured in a trench at one side of the field plots touching the first plant in the row. We used the root counting method on a grid with square cells of 0.0025 m^2 (Bohm, 1979; Tardieu, 1988; Tardieu and Manichon, 1986).

Electrical Resistivity Tomography

Electrical resistivity measurements were conducted using a ten-channel Syscal Pro resistivity meter (IRIS instruments, France) in combination with a strip box to which we connected 54 cables leading to individual electrodes attached by crocodile clips. The electrodes were installed permanently in plots Ba, T1, T4, and T6 of R3 in a line along the slope and inserted at three depths: 36 electrodes at the 5-cm depth, 9 at 25 cm, and 9 at 50 cm (see Fig. 1). The electrodes were stainless steel rods insulated using heat-shrink tubing leaving the 5-cm bottom sharpened ends free as electrode. The horizontal distance between electrodes at 5-, 25-, and 30-cm depth were 33, 132, and 132 cm, respectively.

Once per day, a combination of dipole–dipole and Wenner measurements were performed in each plot consisting of 1694 unique quadrupoles with a measurement time of approximately 1 h per plot. We used this measurement protocol since it was the most promising among tested arrays during a synthetic experimental design study (Garré et al., 2012). During the ERT measurements, TDR probes were disconnected to avoid current losses through the TDR multiplexers.

We used the open source code Gimli (Günther et al., 2006, Rücker et al., 2006) to perform a 2.5-D inversion to image the soil bulk electrical conductivity. A finite element method was used to solve the Poisson equation (forward problem):

$$\nabla\cdot(\mathbf{EC_b}\nabla\varphi)-\nabla\cdot\boldsymbol{j}_s=0 \qquad [1]$$

where $\mathbf{EC_b}$ is the bulk soil electrical conductivity (S m^{-1}), φ the electric potential (V), and $\boldsymbol{j}_s$ is the source current density (A m^{-2}). The forward simulation domain was 100 m wide and 50 m deep, and the surface topography was based on 14 measurements along the slope (1-m distance). No-flow boundary conditions were applied on all boundaries. The inversion was performed using an error-weighted, smoothness constrained Occam type algorithm. The algorithm minimizes an objective function ($\mathbf{\Phi}$) composed of a data functional ($\mathbf{\Phi}_d$), a regularization parameter (λ) and a model functional ($\mathbf{\Phi}_m$) (Günther et al., 2006):

$$\mathbf{\Phi}=\mathbf{\Phi}_d+\lambda\mathbf{\Phi}_m\rightarrow\min \qquad [2]$$

in which $$\mathbf{\Phi}_d(\mathbf{m})=\left\|\mathbf{D}\left[\mathbf{d}-\mathbf{f}(\mathbf{m})\right]\right\|_2^2 \qquad [3]$$

and $$\mathbf{\Phi}_m(\mathbf{m})=\left\|\mathbf{C}\left(\mathbf{m}-\mathbf{m}^0\right)\right\|_2^2 \qquad [4]$$

$\mathbf{m}$ is the model vector, $\mathbf{d}$ is the data vector that represent log transformed measured resistances, $\mathbf{f}(\mathbf{m})$ is the forward response of the model, and $\mathbf{m}^0$ is a starting or reference model. $\mathbf{D}$ is the data weighting matrix, i.e., a diagonal matrix with inverse errors on the main diagonal, and $\mathbf{C}$ is the model smoothness matrix. The individual timesteps were processed independently, since time lapse approaches produced solutions with a higher residual than independent inversions.

We assumed, as in Koestel et al. (2009), that the data error of a single measurement can be approximated using a Gaussian error model that comprises an absolute resistance error component, $\alpha(\Omega)$, and a relative component, β. These two components were calculated for the ensemble of data (= all timesteps and all quadrupoles together). The differences between normal and reciprocal measurements were collected for different intervals of R_i. For each of the intervals, the standard errors of these differences were calculated and this was used to obtain an estimate of the error for a measurement with a resistance R_i. The resistance R_i is the average of the normal and reciprocal measurement of the quadrupole. When an average of normal and reciprocal measurements is used in the inversion, this error must be divided by square root of 2. The relative error, ε_i (–), on the measured resistance, R_i, of each single data

Table 1. Coeffients α and β of the error model for the inversion of the resistivity data for each field plot.

	α	β
	Ω	
BaR3	0.0058	0.0112
T1R3	0.0060	0.0158
T4R3	0.0053	0.0072
T6R3	0.0041	0.0071

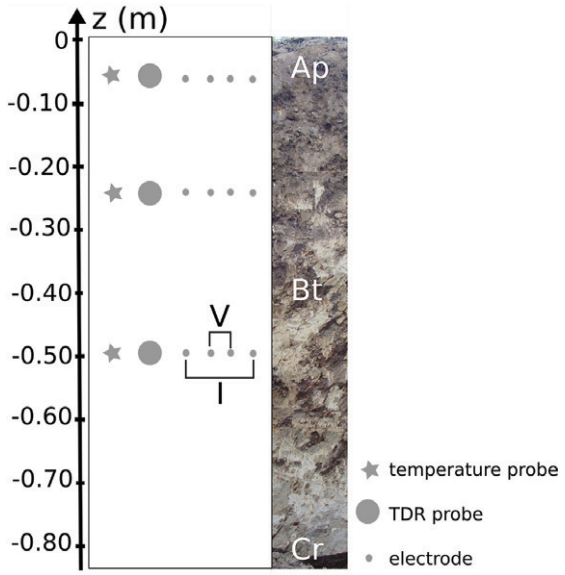

Fig. 2. Scheme of calibration pit: equipment and soil profile. The horizontal distance between the electrodes was 10 cm.

point is a good approximation of the error of the log transformed resistance d_i, which is then used in the inversion algorithm:

$$\varepsilon_i = \frac{(\alpha + \beta R_i)/\sqrt{2}}{R_i} \quad [5]$$

The error model fit was done after application of a course data filter. We estimated the data error for the ensemble of all timesteps and all quadrupoles following the procedure as in Koestel et al. (2008). Table 1 gives an overview of the coefficients α and β for each of the four plots. After the error model estimation, the data were filtered so that the difference between normal and reciprocal measurement was never larger than 0.8R.

Temperature probes, TDR probes, and electrodes were inserted at 5-, 25-, and 50-cm depth in a vertical wall of a calibration trench (1-m depth) in an area of bare soil below field plot T4R3. Three soil horizons were identified in the calibration pit: an Ap (0–25 cm), a Bt (26–80 cm), and Cr (>80 cm) (see Fig. 2). However, it must be noted that the transition between Ap and Bt was not clear and the depth also varied along the profile pit. Soil temperature, water content, and resistance were logged twice a day.

The electric field in the calibration pit caused by the current electrodes is limited by two surfaces: the vertical wall of the calibration pit, of which the effect is included in the classical formula for a hemispherical shell in a half space, and the horizontal soil surface. This additional horizontal surface was taken into account for the resistivity calculations using the method of mirror current injections. The resulting geometric factors for the Wenner array at 5-, 25-, and 50-cm depth are, respectively, 0.4134, 0.6155, and 0.6265 m.

Data Processing Temperature Correction

There are two distinct effects of temperature on soil bulk electrical conductivity. A temperature change has an effect on the mobility of the ions in the soil solution. An increase in soil temperature implies a decrease of the viscosity and thus an increase of the ion mobility, a connection described by the Stokes–Einstein equation. Most of the current models for temperature correction of electrical resistivity correct for this first factor. Depending on the mineralogy of the soil and the solubility of the minerals, there can be an effect of temperature on the total dissolved solids (TDS) in the pore water, which is an irreversible process. We assume that the second effect is only of minor importance in our field experiment. The resistivity data of this study are corrected for temperature using the following relationship (Campbell, 1949) with $c = 0.02$

$$EC_{b,25} = \frac{EC_b}{[1 + \alpha(T - 25)]} \quad [6]$$

For an overview of temperature correction models, consult Ma et al. (2011).

The soil temperature profile $T(z,t)$ during the measurements was predicted using the heat flow equation:

$$\frac{\partial T}{\partial t} = K_T \frac{\partial^2 T}{\partial z^2} \quad [7]$$

The top boundary condition (BC) was set using the temperature measured at 5 cm depth under the three different crops during the whole growing season.

We derived the soil thermal properties based on average daily temperature changes in the soil as described in Jury and Horton (2004, p.187–191). We used the 9-d time series of soil temperature at five depths to derive the damping depth of the soil, which is necessary to derive K_T in Eq. [7]:

$$\Delta T = T_{max} - T_{min} = 2A\exp\left(\frac{z}{d}\right) \text{and } K_T = \pi d^2 \quad [8]$$

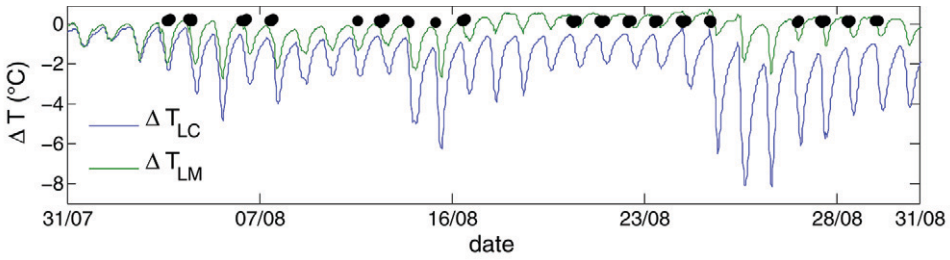

Fig. 3. Difference in soil temperature for Leucaena and Chili (ΔT_{LC}) and for Leucaena and Maize (ΔT_{LM}). Timing of electrical resistivity tomography (ERT) measurements is indicated with black dots.

K_T (cm^2 d^{-1}), the apparent soil thermal diffusivity, was derived from the damping depth d (cm) using Eq. [8] and that d was derived from fitting the first part of Eq. [8]. In addition, A (°C) is the average amplitude of the sine wave of the diurnal temperature and z (cm) is the soil depth. $T_{max(z)} - T_{min(z)}$ were calculated from the 9-d time series of soil temperature during which the daily averaged soil temperature did not change considerably. As Fig. 3 shows, the temperature under the different crops varies by up to several degrees.

Conversion of Bulk Electrical Conductivity to Water Content

As in Michot et al. (2003), we used soil moisture and temperature corrected bulk electrical conductivity data at three depths of a nearby calibration pit to establish a relationship between the two variables. During the field experiment, 56 data points were collected at three depths. Inspection of the data showed that the first two depths could be joined since they had a similar behavior and thus belonged to the same soil horizon. It must be noted that the second sensor was located close to the horizon boundary as identified by the profile description (see above). Based on the results of the calibration relation and keeping in mind that the soil horizon boundary was unclear in the field, we decided that the horizon boundary must have been between the two sensors with contrasting behavior, i.e., around 40 cm. It is clear that the horizon boundary is not exact and that there is uncertainty about the relation between the bulk soil electrical conductivity and the soil moisture content in the neighborhood of the boundary between the two layers with different calibration relations.

Subsequently, we fit a simplified Waxman and Smits (W–S) model (Waxman and Smits, 1968) to the data:

$$\mathrm{WC} = \left\{ \frac{\left(\mathrm{EC}_{b,25} - b\right)}{a} \right\}^{1/n} \qquad [9]$$

where WC is the volumetric water content, $\mathrm{EC}_{b,25}$ is the bulk soil electrical conductivity at 25°C. In addition, a, b (S m^{-1}) and n are fitting parameters. This equation assumes that the surface conductivity of the soil is not affected by pore water salt concentration or water content. The parameters in the simplified W–S function can thus still be interpreted in a physical manner: a is affected by the pore water conductivity and b by the soil surface conductivity, both in combination with the porosity. Figure 4 shows the data points and the fitted calibration function for the two horizons. The optimized parameters are a = 0.23, b = 0.0036 S m^{-1}, and n = 2.28 for the first horizon (0–40 cm) [root-mean-square error (RMSE) = 0.0011] and a = 0.16, b = 0.0041 (S m^{-1}), and n = 2.81 for the second horizon (40–80 cm) (RMSE = 0.0008). The parameter values a and b are smaller than the values for an orthic Luvisol reported in Garré et al. (2011), whereas n is larger than those of most soil layers in that work. The functions also lie within the range of the data gathered by Vanderborght et al. (2012).

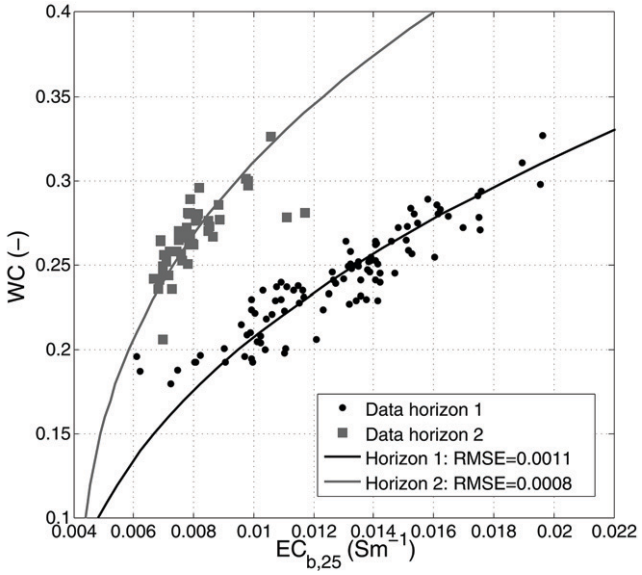

Fig. 4. Fit of the simplified Waxman and Smits model to data of horizon 1 (Ap) and horizon 2 (Bt) in the calibration pit.

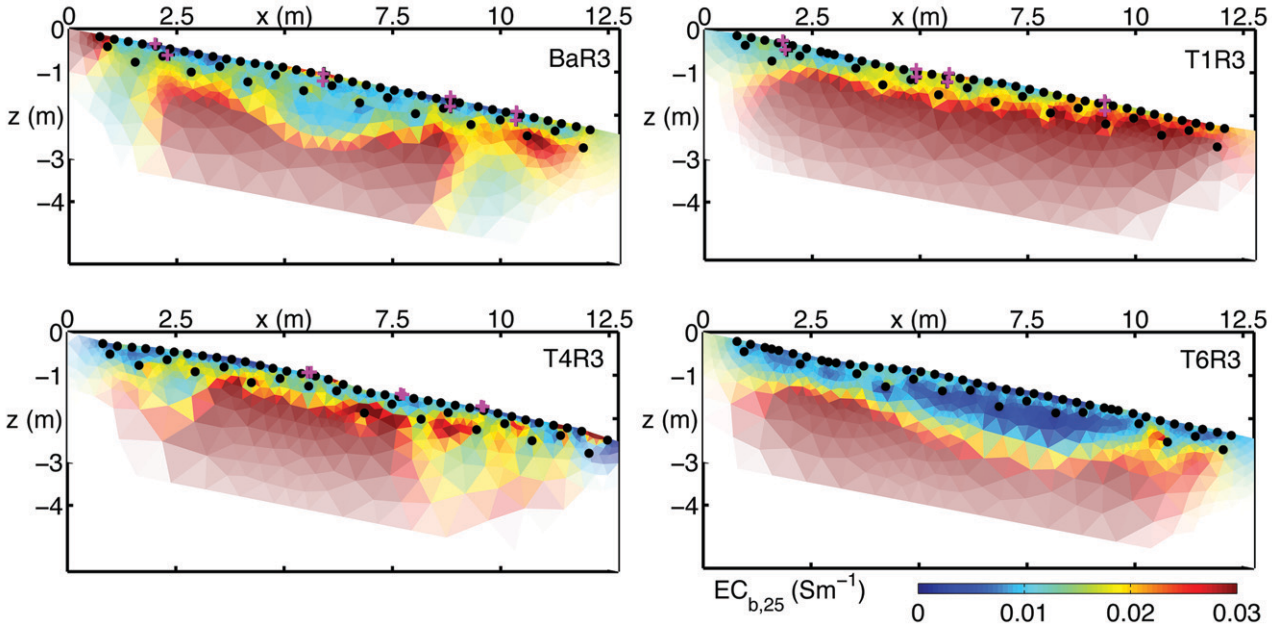

Fig. 5. Temperature corrected bulk electrical conductivity distribution, $EC_{b,25}$ (Sm^{-1}), for treatments BaR3, T1R3, T4R3, and T6R3 on 6 Aug. 2011. Electrodes and time domain reflectometer (TDR) probe locations in the two-dimensional plane are indicated with dots and crosses, respectively. The brightness levels represent decreasing coverage of the electrical resistivity tomography (ERT) data.

Results and Discussion

Structural Information

Figure 5 shows the two-dimensional temperature corrected bulk electrical conductivity distribution on 6 Aug. 2011 (DOY 218) along the slope of four cropping patterns. Two distinct zones emerge from the $EC_{b,25}$ distributions of which we hypothesize that they represent the soil and the (weathered) bedrock. The soil augerings (see supplementary materials) seem to confirm this hypothesis, but it must be noted that the correlation between soil augerings and the EC profile is weak. The inverted EC_b distribution may be used as a proxy for estimation of the distribution of the bedrock in the subsurface. We used as a rough approximation a threshold inverted EC_b of 0.02 S m^{-1} to delineate the bedrock boundary. It should, however, be noted that the imaged EC_b distribution is prone to inversion artifacts resulting from smoothing and low sensitivity but may nevertheless be informative of the subsurface structure. The soil depth is very heterogeneous in all plots. T1R3 and T4R3 have the shallowest soils. Figure 5 also shows that the location of the horizon transitions along the slope is not necessarily parallel to the soil surface. This adds an extra uncertainty about the ranges of depths for which the calibration relationships shown in Fig. 4 can be applied.

Soil Moisture Dynamics under Different Cropping Patterns

Time Series of Water Budget using TDR and ERT

During the ERT campaign, only a few rain events were registered. Two major intervals in which the soil moisture evolves from wet to dry can be defined as shown in Fig. 6: from 30 July to 15 August and from 15 August to 11 September. The air temperature ranged between 20°C and 35°C, with differences between daily minimum and maximum up to 12 degrees. The average soil moisture contents in the first 0.5 m of the four studied plots were highest by the end of July and decreased gradually during the growing season. After the

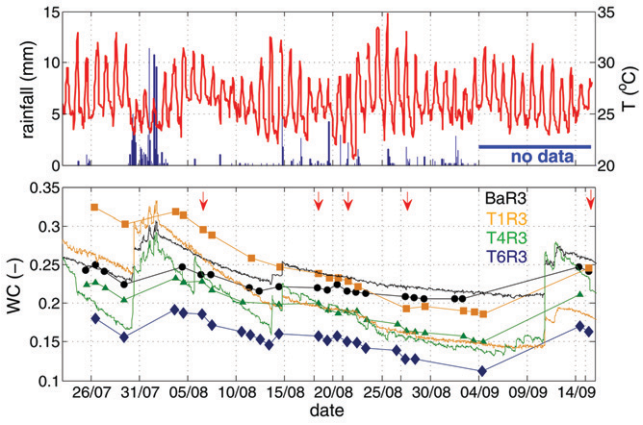

Fig. 6. Hourly rainfall (mm) [blue] and air temperature (°C) [red] during the measurement campaign (top) and average electrical resistivity tomography (ERT)-measured soil moisture content of the first 0.5 m of the soil profile in the ERT plane for BaR3, T1R3, T4R3 and T6R3 (lines with markers) together with the average soil moisture measured by time domain reflectometer [(TDR), (fine lines, bottom)] as an indication of the measured soil moisture changes. The red arrows indicate timeframes later used in Fig. 8.

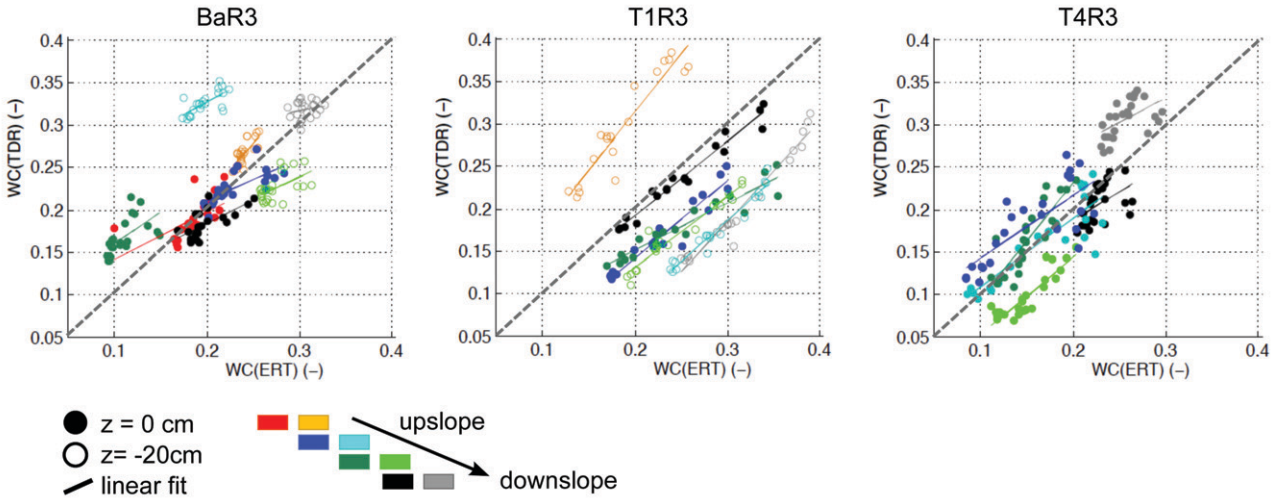

Fig. 7. Scatterplot of water content obtained by electrical resistivity tomography (ERT), WC(ERT), vs. water content obtained by time domain reflectometer (TDR), WC(TDR) during the ERT campaign. Dots of the same color are data belonging to one TDR probe location.

first heavy rains (of the rainy season) in September, the soils were replenished. Unfortunately, the magnitude of the rain showers in September could not be recorded due to a technical problem with the pluviometer of the meteorological station. Additionally, the very local character of rain events made it difficult to use weather data from nearby stations. Both the TDR and ERT data showed that he monocropped maize plot lost most water during the growing season, whereas the bare soil plot showed the least change. The fertilized and unfertilized intercropped plots showed a similar water dynamic throughout the growing season. When comparing the within-plot averaged TDR and ERT derived water contents, it should first be noticed that difference between both remains fairly constant over time. This means that the temporal dynamics of the soil moisture obtained with the two methods is very consistent. When comparing the absolute values of the within-plot averaged TDR and ERT derived soil moisture contents, one must keep in mind that the experimental site was quite heterogeneous, which is also evidence by the spatial variation of EC_b values within and between the different transects (see Fig. 5). First, because of this heterogeneity, the average moisture content derived from 8 TDR probes is uncertain. Note that the standard deviation of the moisture content measured by the different TDR probes within a plot was on average 0.006 for Ba, 0.011 for T1, and 0.008 for T4. Second, the spatial variability is most likely also mirrored in a spatial variability of the relation between EC_b and θ that is more complex than what we account for by using two EC_b–θ relations for a two layer system with fixed layer depths. For instance, despite the fact that the TDR data also suggest higher water contents at the beginning of the monitoring period in plot T1R3 than in the other plots, the high water contents obtained with ERT may be due to the influence of the weathered bedrock on the inverted EC_b values in this plot. The weathered bedrock showed higher EC_b values than the top soil layers and was shallower in plot T1R3 than in the other plots (see Fig. 5).

Next to local monitoring of soil moisture content at a high time resolution, the TDR data can also be used as a ground truth for the water content distribution obtained from ERT. Soil moisture data from TDR, WC(TDR), and local ERT, WC(ERT), during the measuring campaign are depicted in Fig. 7. The TDR probes were not located in the same *xz*-plane as the electrodes. Some differences between data registered by the two methods can thus be expected, given the high heterogeneity of the soil, the stone content and the use of the standard Topp's equation for the TDR data. To be able to retrieve the spatial location of a point in the data cloud, we adopted a two-folded symbology in the image: a dark (most left TDR transect)–light (most right TDR transect) color and a closed (0–0.25-m depth)–open (0.20–0.45-m depth) circle. When talking about left and right, we are looking from the bottom of the plot uphill. As depicted in Fig. 1, we have four locations along the slope with TDRs installed in BaR3. The probes at the left side were installed from 0–0.25 m, the probes at the right from 0.20–0.45 m. In T1R3, the probes at the most left transect were from 0–0.25 and the ones at the most right transect from 0.20–0.45 cm. In T4R3, there were no probes from 0.20–0.45 cm; only from 0–0.25 cm. Two TDR probes did not function well, probably due to damage while installing in the stony soil, and the data were excluded from analysis (no red color in T1R3 and T4R3).

The water contents derived from the deeper TDR probes often show larger differences from the ERT data than the surficial ones, which may be due to the larger heterogeneity in the subsoil and the lateral distance between the TDR probes and the ERT transect. In addition, next to the distance between TDR probes and ERT transect, the fact that the exact location of the transition between soil horizons along the slope is not known and consequently the calibration relation between EC_b and θ may have caused a deviating WC(ERT) for the deeper TDR locations. The temporal dynamics

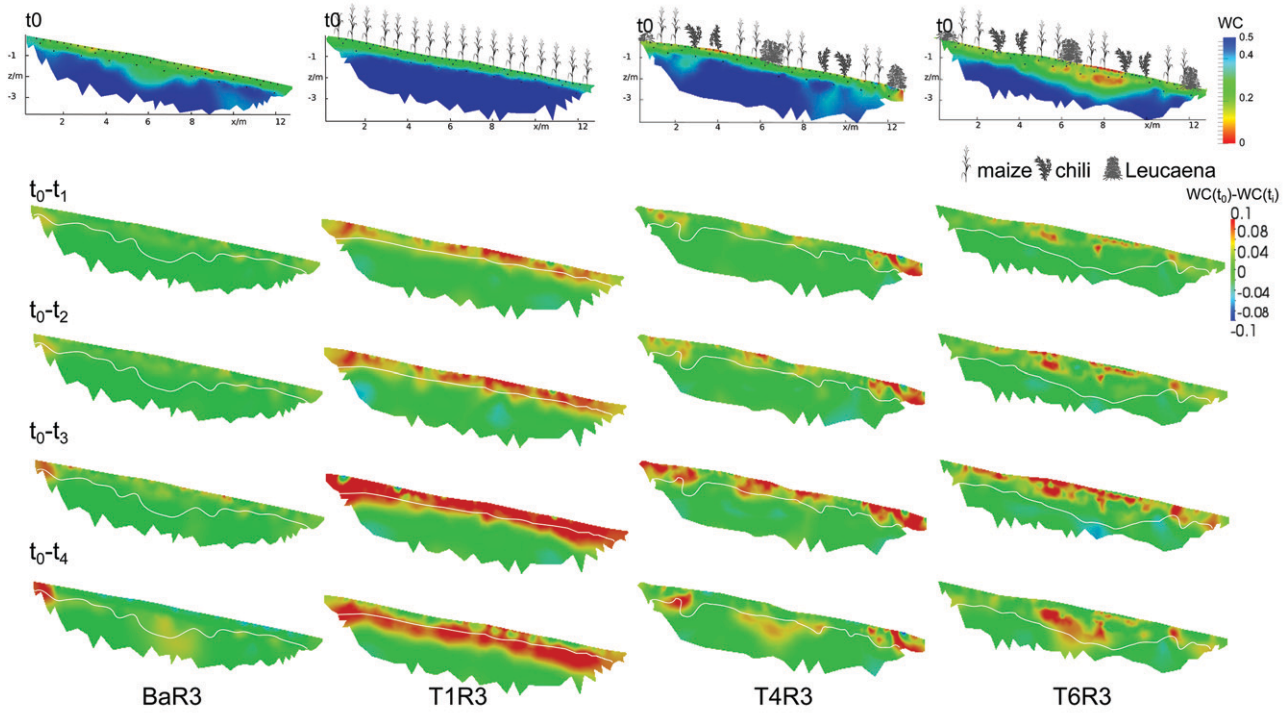

Fig. 8. Derived soil moisture distribution on 6 Aug. 2011 (t0) and distribution of the differences in soil moisture between reference day t0 and 18 August (t1), 21 August (t2), 27 August (t3), and 15 September (t4). The white line represents the transition between soil and weathered bedrock in the two-dimensional plane.

of water contents and its variability with depth, location within the plot, and between plots that is observed in the TDR and ERT data are very similar. This can be concluded from the point clouds in Fig. 7, which correspond with measurements at a certain depth and location, showing a similar spreading along the *x*- and *y*-axes. This means that, even if there is an over- or underestimation of the moisture content by ERT, this difference remains constant over time for most TDR probes and locations.

Both ERT and TDR data showed considerably smaller temporal variations of water contents in the bare soil plot than in the cropped plots. This is especially true for the deeper measurements. In a bare soil, the dynamics of the soil moisture deeper in the soil profile is always considerably smaller than in a cropped soil since there is no root water uptake in a bare soil. It should also be noticed that this difference in soil moisture dynamics between cropped and bare soil is not only visible between the different plots but also within the intercropped plot T4R3. The downslope TDR probes in this plot are installed under the chili plant rows (Fig. 1), which due to the low leaf area index and leaf coverage behave like a bare soil strip. Both ERT and TDR data (gray and black dots) show a much smaller temporal dynamics of soil moisture than the TDR and ERT points located under the maize rows in this plot. Because of scatter, linear regression lines through point clouds of ERT vs. TDR water contents at locations with low temporal soil moisture dynamics are smaller than one. However, for the cropped field plots, the temporal range of water contents is considerably larger and the regression lines for locations that show a considerable temporal dynamics have a slope that is close to one (see Fig. 7 for T1R3 and T4R3). This indicates that ERT data can be used to derive water content changes over time and the spatial variability of these changes within a field.

Spatial Distribution of Water Depletion

Figure 8 shows the ERT-derived soil moisture distribution on 6 Aug. 2011, which is used in this figure as a reference timeframe, t0. Again, we see two distinct zones: soil and weathered bedrock. The water content in this second zone should not be interpreted, since we could not measure a pedo-physical relationship in the bedrock. However, we do show this part of the section, to investigate whether the crops and/or hedge also accessed water stored in the weathered bedrock. The volumetric water content in the soil at t0 ranges between 20 and 30%. Soil moisture changes from the reference timeframe t0 are also shown in Fig. 8. Between the reference timeframe t0 and t3, only one small rain event occurred. The concurrent differences show us the effect of this long drying phase on soil moisture changes in the four cropping patterns (with red colors showing water depletion relative to t0). Timeframe t4 comes immediately after a few days with rain. The images representing t4–t0 show the infiltration of water at the surface (thin green band at the surface).

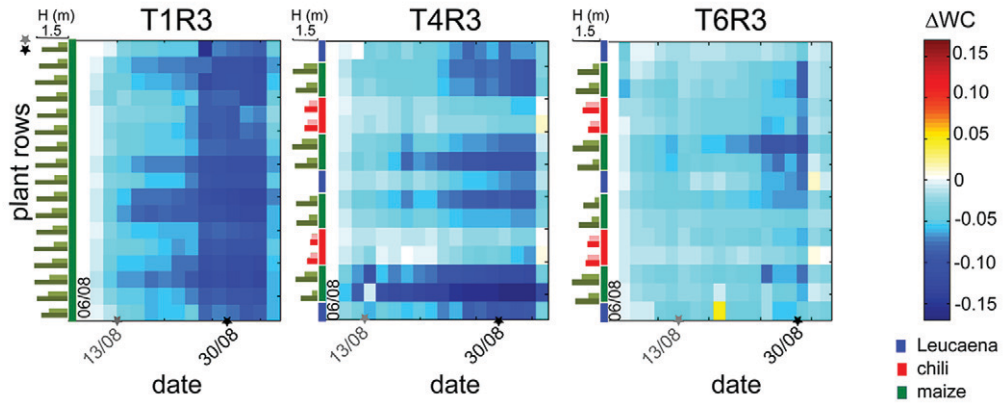

Fig. 9. Average water depletion (ΔWC) under crop rows obtained from electrical resistivity tomography (ERT) data between $z = 0$ and $z = -0.8$ m for three cropping patterns: monocropping (T1R3), hedgerow intercropping with fertilizer (T4R3), and hedgerow intercropping without fertilizer (T6R3). Average plant height per row of three plants closest to the ERT transect is indicated at the left side of the ΔWC-graph of each treatment for $t = 13$ Aug. 2011 and $t = 30$ Aug. 2011.

There is a clear difference in water depletion patterns for the different cropping patterns. The bare soil plot (BaR3) has only a minor water loss as compared to the others and the water loss occurs mainly at the soil surface. The soil moisture changes for this plot are merely due to evaporation and soil water redistribution. In the monocropped maize plot (T1R3) a clear uptake pattern emerges which coincides with the plant rows. This result is similar to the observations made by Beff et al. (2012) under wetter conditions in a temperate climate and on flat land. Srayeddin and Doussan (2009) measured a more heterogeneous water depletion pattern. In our study, water depletion gradually moved downward, to the fringe of the soil domain and even slightly in the weathered bedrock. The intercropped fields (T4R3 and T6R3) resulted in very heterogeneous uptake patterns. The maize plants had the highest depletion rates per cell of the mesh, whereas the Leucaena hedge had a more dispersed depletion pattern, which finally reached a little bit deeper (in the weathered bedrock) than the one of the maize plants in this plot. Leucaena is not known for the development of deep roots. Previous studies (Jonsson et al., 1988, Toky and Bisht, 1992) investigating the root system of Leucaena report that the plant had a similar rooting depth as maize and developed most of its root biomass in the first 30 cm of the soil profile. From our root counting data, we could see that Leucaena developed indeed most of its biomass in the same depth region as the maize [$z = (0,-0.5$ cm)], but it also developed deeper roots which was not observed for the maize plants. In addition, Leucaena developed its root mass laterally into the rooting zone of the maize rows (not shown). The chili plants in the intercropped fields hardly take up water as compared to the other crops. It must be noted that the Chili was not vigorous due to several infestations. Several fungal diseases and insects caused yield loss. Cercospora leaf spot (*Cercospora capsici* Heald & F.A. Wolf) resulted in almost complete defoliation. Another major problem was crown rot or basal stem rot caused by *Phytophthora capsici* Leonian. Powdery mildew [*Leveillula taurica* (Lév.) G. Arnaud], moreover, was seen during the cool season. As for insects, thrips and aphids were the main problem for heavy damage of the chili plants. Finally, we can see a rewetting front in the top soil after the rainfall events at the end of the monitoring campaign (last row Fig. 8).

Crop Behavior

Different water depletion patterns emerge when comparing the overall soil moisture difference distributions of different cropping patterns and crops within one treatment (Fig. 8). Figure 9 shows the average water depletion under [$z = (0$ m,-0.8 m)] each crop type during the growing season. The monocropped maize treatment clearly used more water than the other treatments. Some rows reached a difference of more than 20% volumetric water content between the beginning and the end of August. The intercropped plots were much more heterogeneous in terms of water depletion. Maize was the largest water consumer, followed by the Leucaena hedges. The Leucaena in the middle of T6R3 and the one at the top of T4R3 have depletion rates that only differ a little from the neighboring maize rows. The other hedges showed less depletion immediately under the row as compared to the neighboring maize. The chili plants used markedly less water than the other crops. This pattern was visible in both the fertilized (T4R3) and the unfertilized (T6R3) treatments. However, in the plot without fertilization, the water depletion was much lower than in the one with fertilizer, even though there is no big difference in plant height. In T4R3, the water loss below the rows closest to the Leucaena hedge was the largest. This could also point at an additional water uptake by the Leucaena roots, which laterally spread out under the first maize row adjacent to the Leucaena hedge. This suggests that there was competition between crop and hedge. In the unfertilized plot, T6R3, this was less clear. The same analysis for $z = [-0.6,-1.2]$ (not shown) confirms the observation from Fig. 8 that at the end of the growing season, there was a decrease in water content in the weathered bedrock layer under the Leucaena hedges. In the intercropped

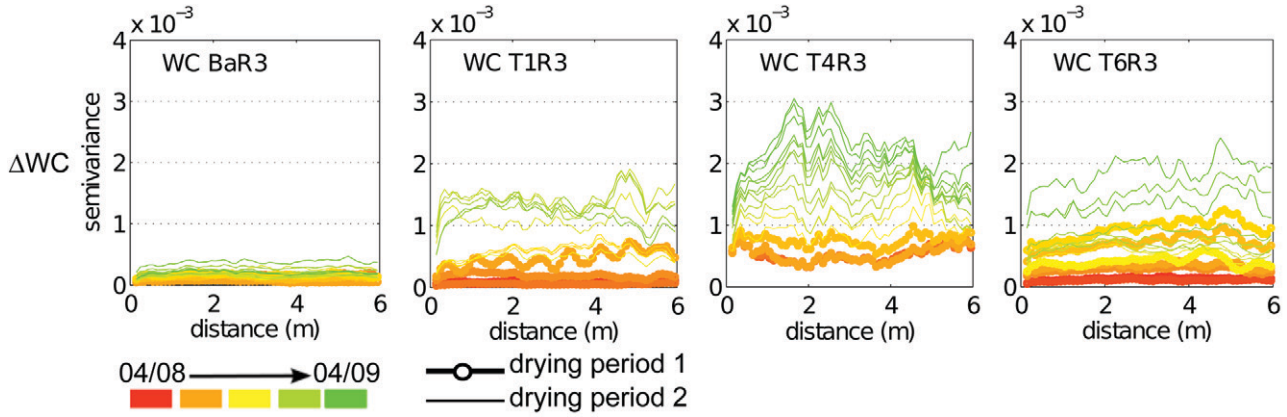

Fig. 10. Experimental semivariograms of the difference of the electrical resistivity tomography (ERT)-measured water content between the distribution at t = 6 Aug. 2011 and the other timesteps (ΔWC) for all four cropping patterns: bare soil (BaR3), monocropped maize (T1R3), hedgerow intercropping with fertilizer application (T4R3), and fertilizer application without fertilizer (T6R3). The calculation was restricted to mesh cells up to 0.4-m depth under the soil surface.

treatments, this was restricted to the Leucaena and neighboring maize plants in the middle of the plot, but in the monocropped plot, water depletion, at this depth, was also visible under some maize rows.

Spatial Statistics

As shown in Garré et al. (2012), experimental semivariograms of the soil moisture distributions demonstrate whether and which systematic spatial structures are present in the water content distribution due to the agricultural treatment. Because spatial variation in absolute moisture data is influenced by bedrock depth, we focus instead on the soil moisture differences relative to the 6 August base dataset. The experimental semivariograms for each treatment (Fig. 10) show clear differences between the four cropping patterns, which is due to the crop choice and alignment.

The semivariance of the bare soil plot is markedly lower than the others. The highest semivariance is found in the fertilized intercropped plot T4R3. In addition, structures caused by the crops rows emerge during a period of drying. In T1R3, the maize row distance of 0.75 m becomes visible after drying (lowest semivariance at lags of 0.75 m and multiples of 0.75 m). It must be noted that the shape of the semivariograms of mono- and intercropped plots is very similar to the ones of the virtual ERT experiment of Garré et al. (2012). The dotted lines represent a first drying period and the lines a second drying period after a small rain event in the middle of August. The rainfall smoothed out the spatial structures, which were reestablished again after drying.

Uncertainty Concerning Location Soil Horizon Interfaces

As mentioned above, the location of horizon interfaces is uncertain in complex field situations, which results in an additional uncertainty for the use of horizon-specific calibration relationships WC = f(EC). In our case, soil profile description and calibration data gave differing information about horizon thickness. The profile description put the horizon boundary at 0.25 m depth, whereas the calibration data suggested this boundary should be deeper down in the profile. Figure 11 shows again the soil moisture data from TDR, WC(TDR), and local ERT, WC(ERT) for the TDR probes at 0.20–0.45-m depth as in Fig. 7. However, here we show this scatter plot once assuming the horizon boundary is at 0.20 m and once assuming it is at 0.40 m. The latter was the assumption for the analysis throughout the text. The figure shows us that the comparison of ERT and TDR cannot really show us which horizon depth is the best choice. There is a lot of spatial variation in this horizon. In addition, the slopes of the relation between WC(ERT) en WC(TDR) is not much influenced by the different soil horizon boundary. If we now calculate the row-wise water depletion for a depth of the horizon at 20 cm and compare it with the ones for a boundary at 0.40-m depth, we find that the mean difference in water depletion and its standard deviation over both space and time is mean 0.0030 (SD = 0.0027) for T1, 0.0024 (SD = 0.0024) for T4 and 0.0029 (SD = 0.0026) for T6. This suggests that the impact of uncertainty about the soil horizon depth on estimated water depletion is not so large when compared with the soil horizon depth.

Conclusions

We successfully monitored soil moisture distributions and changes in the field under different cropping patterns with ERT. In addition, the distribution of electrical conductivities showed the existence of two main structural entities in the profiles and revealed the heterogeneity of the soil depth across the research plots. The soil moisture status of the different treatments and the change thereof was measured; in addition, whereas the average soil moisture change of the treatments was similar, clear differences in depletion patterns were recognized making use of the spatial

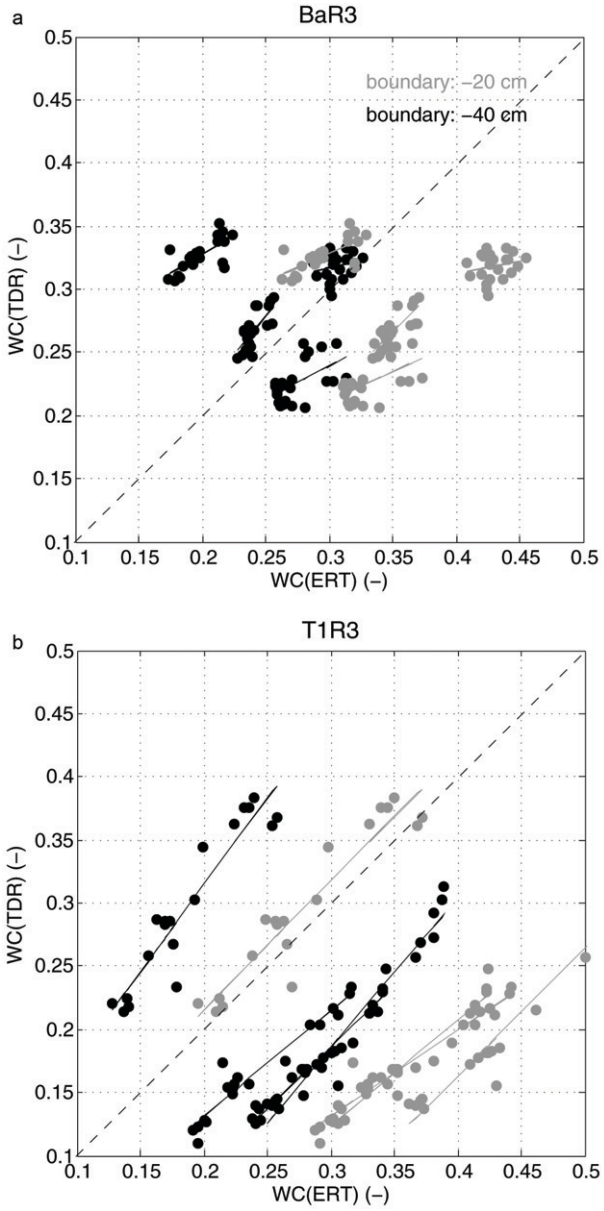

Fig. 11. Scatterplot of water content obtained by electrical resistivity tomography (ERT), WC(ERT), vs. water content obtained by time domain reflectometer (TDR), WC(TDR) for the TDR probes located at 0.2–0.45-m depth for two cases: the horizon boundary at z = −0.2 cm (gray) and the boundary at z = −0.4 cm (black).

information provided by the ERT. This knowledge was crucial to understand the validity of the applied calibration relationship to convert measured bulk electrical conductivity to soil water content. It became clear that at places with shallow soil, we did not have a calibration relationship for the weathered bedrock and that in these areas, absolute values had to be used with caution. However, even though quantitative information about this area lacked, changes could be registered, which would have been impossible with conventional soil moisture sensors.

The greatest value of the ERT data from the field lies in the possibility to investigate spatial and temporal patterns. Comparison of water depletion under distinct crop types showed that the depth of the depletion of the chili culture was much less than that of maize and Leucaena. Moreover, local differences in magnitude of depletion were visible comparing the fertilized and unfertilized treatment. Measurement of increased depletion under the maize rows close to the hedges pointed toward competition for water between the two plants, which was supported by the observation of the presences of roots of both plants in this region. Finally, experimental semivariograms allowed us to investigate the variability of soil moisture and soil moisture changes and its spatial distribution. This technique showed that variability of the measured soil moisture was largely influenced by the soil heterogeneity. The use of semivariograms of soil moisture change instead of absolute soil moisture allowed de-trending the data and quantifying the crop and treatment effects on the spatial variability of water depletion. The use of spatial analysis thus allows extracting very valuable information from ERT data, which is unavailable when using point measurements of soil moisture.

Acknowledgments

We would like to thank the KULeuven for funding this OT project and the colleagues of the University of Hohenheim (Thomas Hilger, Georg Cadisch, Khalid Hussain) and Kasetsart University (Thanuchai Kongkaew, Chalemchart Wongleecharoen, Wattanai Omsunrarn, Channarong Khetdan) for their support during field experiments and discussions. The ERT equipment was kindly provided by Forschungszentrum Jülich GmbH. Finally, we would like to express our profound gratitude to Prof. Thanuchai Kongkaew, who passed away last year on 16 Feb. 2012. Thanks to his perseverance, we were able to conduct this study at the research site in Ratchaburi.

References

Aerts, R., R. Boot, and P. van der Aart. 1991. The relation between above- and belowground biomass allocation patterns and competitive ability. Oecologia 87:551–559 10.1007/bf00320419. doi:10.1007/BF00320419

Agus, F., D.K. Cassel, and D.P. Garrity. 1997. Soil-water and soil physical properties under contour hedgerow systems on sloping oxisols. Soil Tillage Res. 40:185–199. doi:10.1016/S0167-1987(96)01069-0

Amato, M., G. Bitella, R. Rossi, J.A. Gómez, S. Lovelli, and J.J.F. Gomes. 2009. Multi- electrode 3D resistivity imaging of alfalfa root zone. Eur. J. Agron. 31:213–222. doi:10.1016/j.eja.2009.08.005

Beff, L., T. Günther, B. Vandoorne, V. Couvreur, and M. Javaux. 2012. Three-dimensional monitoring of soil water content in a Maize field using Electrical Resistivity Tomography. Hydrol. Earth Syst. Sci. Discuss. 9:8535–8578. doi:10.5194/hessd-9-8535-2012

Bohm, W. 1979. Methods of studying root systems. Springer-Verlag, Berlin.

Campbell, R.B. 1949. Change of electrical conductivity with temperature and the relation of osmotic pressure to electrical conductivity and ion concentration for soil extracts. Soil Sci. Soc. Am. J. 13:66–69. doi:10.2136/sssaj1949.036159950013000C0010x

Cassiani, G., N. Ursino, R. Deiana, G. Vignoli, J. Boaga, M. Rossi, M.T. Perri, M. Blaschek, R. Duttmann, S. Meyer, R. Ludwig, A. Soddu, P. Dietrich, and U. Werban. 2012. Noninvasive monitoring of soil static characteristics and dynamic states: a case study highlighting vegetation effects on agricultural land. Vadose Zone J. 11. doi:10.2136/vzj2011.0195.

Craswell, E.T., A. Sajjapongse, D.J.B. Howlett, and A.J. Dowling. 1997. Agroforestry in the management of sloping lands in Asia and the Pacific. Agrofor. Syst. 38:121. doi:10.1023/A:1005960612386

Danso, S.K.A., G.D. Bowen, and N. Sanginga. 1992. Biological nitrogen fixation in trees in agro-ecosystems. Plant Soil 141:177–196 10.1007/bf00011316. doi:10.1007/BF00011316

Dercon, G., J. Deckers, J. Poesen, G. Govers, H. Sánchez, M. Ramírez, R. Vanegas, E. Tacuri, and G. Loaiza. 2006. Spatial variability in crop response under contour hedgerow systems in the Andes region of Ecuador. Soil Tillage Res. 86: 15–26. doi: 10.1016/j.still.2005.01.017.

Everson, C.S., T.M. Everson, and W. Niekerk. 2009. Soil water competition in a temperate hedgerow agroforestry system in South Africa. Agrofor. Syst. 75:211–221. doi:10.1007/s10457-008-9174-x

FAO/ISRIC/ISSS. 1998. World reference base for soil resources. International Society of Soil Science, Rome.

Garré, S., T. Günther, J. Diels, and J. Vanderborght. 2012. Evaluating experimental design of ERT for soil moisture monitoring in contour hedgerow intercropping systems. Vadose Zone J. 11(4).

Garré, S., M. Javaux, J. Vanderborght, L. Pages, and H. Vereecken. 2011. Three-dimensional electrical resistivity tomography to monitor root zone water dynamics. Vadose Zone J. 10:412–424. doi:10.2136/vzj2010.0079

Günther, T., C. Rücker, and K. Spitzer. 2006. Three-dimensional modelling and inversion of DC resistivity data incorporating topography- II. Inversion. Geophys. J. Int. 166:506–517. doi:10.1111/j.1365-246X.2006.03011.x

Hairiah, K., M. Van Noordwijk, and G. Cadisch. 2000a. Crop yield, C and N balance of three types of cropping systems on an Ultisol in Northern Lampung. NJAS-Wageningen. J. Life Sci. 48: 3–17. doi: 10.1016/s1573-5214(00)80001–9.

Hairiah, K., M. Van Noordwijk, and G. Cadisch. 2000b. Quantification of biological N2 fixation of hedgerow trees in Northern Lampung. NJAS- Wageningen. J. Life Sci. 48:47–59 10.1016/s1573–5214(00)80004–4.

Hauser, S., L. Norgrove, B. Duguma, and E. Asaah. 2005. Soil water regime under rotational fallow and alternating hedgerows on an Ultisol in southern Cameroon. Agrofor. Syst. 64:73–82. doi:10.1007/s10457-005-2442-0

Högberg, P., and M. Kvarnström. 1982. Nitrogen fixation by the woody legume Leucaena leucocephala in Tanzania. Plant Soil 66:21–28. doi:10.1007/BF02203398

Imo, M., and V.R. Timmer. 2000. Vector competition analysis of a Leucaena-maize alley cropping system in western Kenya. For. Ecol. Manage. 126:255–268. doi:10.1016/S0378-1127(99)00091-2

Jonsson, K., L. Fidjeland, J. Maghembe, and P. Högberg. 1988. The vertical distribution of fine roots of five tree species and maize in Morogoro, Tanzania. Agrofor. Syst. 6:63–69. doi: 10.1007/bf02220109.

Jury, W., and R. Horton. 2004. Soil physics. 6th ed. John Wiley & Sons, Hoboken, NJ.

Khedari, J., A. Sangprajak, and J. Hirunlabh. 2002. Thailand climatic zones. Renew. Energy 25:267–280. doi:10.1016/S0960-1481(01)00005-2

Koestel, J., A. Kemna, M. Javaux, A. Binley, and H. Vereecken. 2008. Quantitative imaging of solute transport in an unsaturated and undisturbed soil monolith with 3-D ERT and TDR. Water Resour. Res. 44:17. doi:10.1029/2007WR006755

Koestel, J., J. Vanderborght, M. Javaux, A. Kemna, A. Binley, and H. Vereecken. 2009. Non-invasive 3D transport characterization in a sandy soil using ERT I: Investigating the validity of ERT-derived transport parameters. Vadose Zone J. 8:711–722. doi:10.2136/vzj2008.0027

Lal, R. 1989. Agroforestry systems and soil surface management of a tropical alfisol. Agrofor. Syst. 8:97–111 10.1007/bf00123115. doi:10.1007/BF00123115

Ma, R., A. McBratney, B. Whelan, B. Minasny, and M. Short. 2011. Comparing temperature correction models for soil electrical conductivity measurement. Precis. Agric. 12:55–66. doi:10.1007/s11119-009-9156-7

Michot, D., Y. Benderitter, A. Dorigny, B. Nicoullaud, D. King, and A. Tabbagh. 2003. Spatial and temporal monitoring of soil water content with an irrigated corn crop cover using surface electrical resistivity tomography. Water Resour. Res. 39:1138–1143. doi: 10.1029/2002WR001581

Michot, D., A. Dorigny, and Y. Benderitter. 2001. Determination of water flow direction and corn roots-induced drying in an irrigated Beauce CALCISOL, using electrical resistivity measurements. C. R. Acad.Sci. Ser. II 332: 29–36.

Morgan, R.P.C. 2004. Soil erosion and conservation. Wiley–Blackwell, New York.

Narain, P., R.K. Singh, N.S. Sindhwal, and P. Joshie. 1998. Water balance and water use efficiency of different land uses in western Himalayan valley region. Agric. Water Manage. 37: 225–240. doi:10.1016/s0378- 3774(98)00047-x.

Pansak, W., G. Dercon, T. Hilger, T. Kongkaew, and G. Cadisch. 2007. 13C isotopic discrimination: A starting point for new insights in competition for nitrogen and water under contour hedgerow systems in tropical mountainous regions. Plant Soil 298:175–189. doi:10.1007/s11104-007-9353-y

Pansak, W., T.H. Hilger, G. Dercon, T. Kongkaew, and G. Cadisch. 2008. Changes in the relationship between soil erosion and N loss pathways after establishing soil conservation systems in uplands of Northeast Thailand. Agric. Ecosyst. Environ. 128:167–176. doi:10.1016/j.agee.2008.06.002

Rücker, C., T. Günther, and K. Spitzer. 2006. Three-dimensional modelling and inversion of dc resistivity data incorporating topography- I. Modelling. Geophys. J. Int. 166:495–505. doi:10.1111/j.1365-246X.2006.03010.x

Srayeddin, I., and C. Doussan. 2009. Estimation of the spatial variability of root water uptake of maize and sorghum at the field scale by electrical resistivity tomography. Plant Soil 319:185–207. doi:10.1007/s11104-008-9860-5

Sun, H., Y. Tang, and J. Xie. 2008. Contour hedgerow intercropping in the mountains of China: A review. Agroforestry Syst. 73:65–76. doi:10.1007/s10457–008- 9113-x.

Tang, Y. 2000. Manual on contour hedgerow intercropping technology. ICIMOD, editor. Katmandu, Nepal.

Tardieu, F. 1988. Analysis of the spatial variability of maize root density. Plant Soil 107:267–272. doi:10.1007/BF02370556

Tardieu, F., and H. Manichon. 1986. Caractérisation en tant que capteur d'eau de l'enracinement du maïs en parcelle cultivée. Une méthode d'étude de la répartition verticale et horizontale des racines. Agronomie 6:345–354. doi:10.1051/agro:19860404

Toky, O.P., and R.P. Bisht. 1992. Observations on the rooting patterns of some agroforestry trees in an arid region of north-western India. Agrofor. Syst. 18:245–263. doi:10.1007/BF00123320

Topp, G.C., J.L. Davis, and A.P. Annan. 1980. Electromagnetic determination of soil water content: Measurements in coaxial transmission lines. Water Resour. Res. 16:574–582. doi:10.1029/WR016i003p00574

Vanderborght, J., J.A. Huisman, J. van der Kruk, and H. Vereecken. 2012. Geophysical methods for field-scale monitoring of flow and transport in the root zone. Non-invasive methods for soil-plant investigations. SSSA, Madison, WI.

Waxman, M.H., and L.J.M. Smits. 1968. Electrical conductivities in oil-bearing shaly sands. Soc. Pet. Eng. J. 8:107–122.

Werban, U., S.A. al Hagrey, and W. Rabbel. 2008. Monitoring of root-zone water content in the laboratory by 2D geoelectrical tomography. J. Plant Nutr. Soil Sci. 171:927–935.